Plasma Measurements in High Intensity Electron Beam Diodes

M.D. Johnston, M.L. Kiefer, and S. Patel, Sandia National Laboratories;
N. Bennett, National Security Technologies, LLC;
D. Welch, Voss Scientific, LLC;
V. Bernshtam, R. Doron, S. Biswas, and Y. Maron, Weizmann Institute of Science

Abstract: Experiments are being performed on the Self-Magnetic Pinch (SMP) electron beam diode on the RITS-6 accelerator at Sandia National Laboratories. This diode produces a tightly focused electron beam (< 3mm diameter) which is incident on a high atomic number bremsstrahlung x-ray converter. Typical diode parameters are 120 kA, 7 MeV, and 70ns current pulse, giving a ~45ns x-ray pulse. Plasmas from contaminants on the electrode surfaces propagate into the A-K vacuum gap, affecting the impedance, x-ray spectrum, and pulse width. These plasmas are measured using diagnostics, which include: spectroscopy, optical imaging, and photon detection; to obtain velocity, density, and temperature information. These parameters are measured both spatially, using multi-fiber arrays, and temporally, using streak cameras and avalanche photodiodes. Plasma densities and temperatures are determined from detailed, time-dependent, collisional-radiative (CT) and radiation transport (RT) models, which include Stark broadening of the hydrogen-alpha transition line and carbon ion line ratios. These results are combined with hybrid PIC/fluid simulations to model the plasma's overall behavior. Densities of up to 10^19 cm-3 have been measured on the electrode surfaces, decreasing by several orders of magnitude both radially and axially across the vacuum gap. Electrode plasma expansion velocities of up to 10 cm/microsecond correlate well with the decreasing impedance profile (~0.5 Ohms/ns) observed during the pulse.

Keywords: electron beam diodes, plasma spectroscopy, pulsed-power, flash x-ray radiography

I. Introduction:

A series of self-magnetic pinch diode shots were taken on the RITS-6 (7.5 MV, 180 kA) accelerator [1] at Sandia National Laboratories during which optical plasma diagnostics were fielded. These diagnostics were fielded to gain a better understanding of plasma formation and propagation in vacuum diodes and their effects on diode performance. The SMP diode (figure 1) consists of a hollow, aluminum cathode and a thin aluminum foil anode. Behind the aluminum foil is positioned a ~1/3 electron range tantalum target used to generate bremsstrahlung x-rays. Electrons accelerated across a short, centimeter wide vacuum gap, are focused to a few millimeters diameter at the target, generating very high MA/cm^2 current densities. As the electrons impinge on the anode, plasma ion species are evolved which accelerate back across the A-K gap, and can cause premature impedance collapse of the diode. Details regarding the operation and performance of this diode, and in particular, the geometry associated with its

operation on RITS when configured with a low (40 Ohms) impedance MITL have been reported [2].

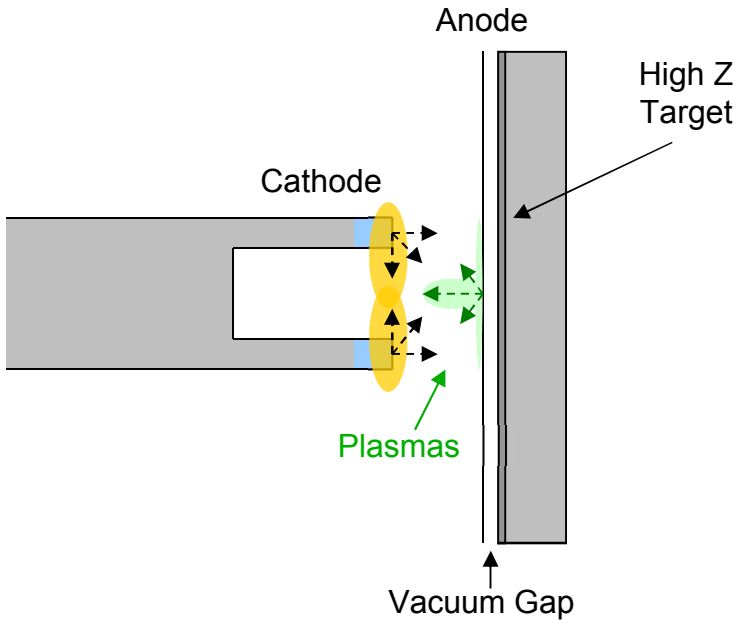

Figure 1. Self-Magnetic Pinch Diode Configuration.

Pinch beam diodes have been studied and used as bremsstrahlung x-ray sources for many years [3-6]. It is well established that ion formation on the anode surface, due to heating from incident electrons, is necessary for pinching the electron beam to the axis [7, 8]. It is generally believed that surface contaminants such as hydrogen, carbon, and oxygen, from water vapor and hydrocarbon residues are the main constituents of these plasmas [9]. What is less understood is the process by which these ions expand into the vacuum gap and their role in the overall impedance behavior of the diode. Similarly, the behavior of ions created within the vacuum gap by processes such as electron impact ionization and charge exchange with neutrals is not well understood. This paper offers experimental evidence of anode plasmas expanding into the A-K gap during the ~70 ns electron beam pulse, and is the first serious attempt to quantify plasma parameters such as temperature and density for these plasmas.

II. Motivation

The self-magnetic pinch diode is a relativistic, pinched electron beam used for flash x-ray radiography. The electron beam is focused to sub-3mm spot sizes onto high atomic number metal targets to produce bremsstrahlung x-rays for flash radiography applications. This type of

diode has been used for many years at the Atomic Weapons Establishment in the United Kingdom, primarily at lower (< 3 MeV) voltages than that of the present RITS-6 accelerator [10]. The motivation for this work is to better understand the role of plasmas in the diode operation at the 7 MeV operating range.

At these voltages, plasmas are rapidly generated on the anode surface as a result of the high on-target current densities (up to 1.5 MA/cm^2). These plasmas appear to be responsible for the steadily increasing current flow in the diode (see figure 2), which results in the diode's characteristic 0.5 Ohms/nanosecond decrease in impedance during a 45ns radiation pulsewidth. The experimentally decreasing diode impedance matches that observed in hybrid PIC/fluid simulations using the LSP code [11]. In addition to this gradual impedance drop, the diode also exhibits a more dramatic impedance drop, with subsequent shortening of the radiation pulse, on some shots, especially those with smaller cathode diameters and shorter A-K gaps. Figure 2 shows an example of the diode current and x-ray dose for two shots listed as "good" and "bad". The "good" shot is representative of what is normally seen on a standard SMP shot. The "bad" shot shows increasing current beginning around 50ns along with a subsequent shortening of the radiation pulse. One of the main goals of the plasma diagnostics is to better understand the role of plasmas in both the normal operation of the diode, as well as during these anomalous events.

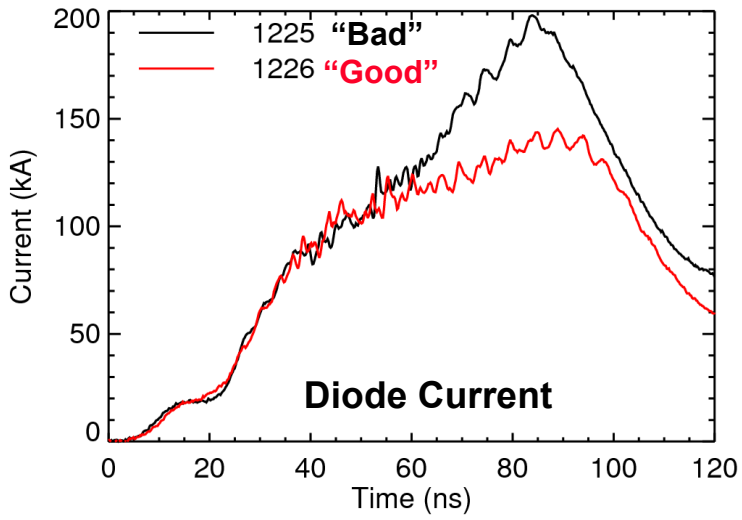

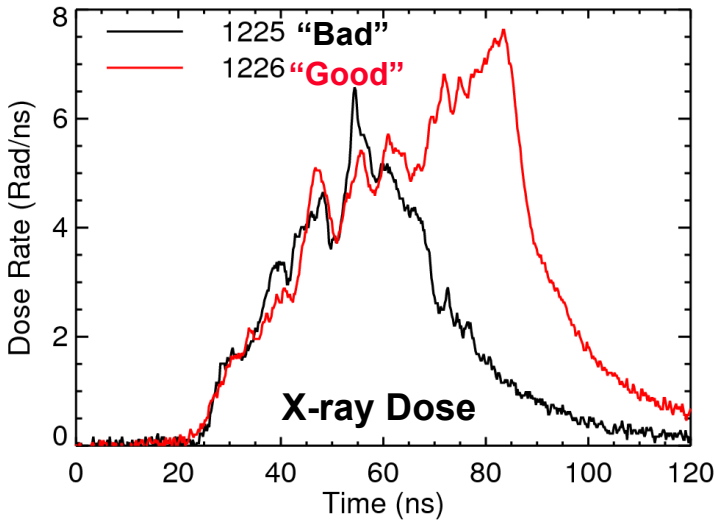

Figure 2. a) Example of diode currents for "good" and "bad" SMP shots. b) Example of x-ray output for "good" and "bad" SMP shots.

Simulations indicate that the direction of ions backstreaming from the anode to the cathode is important in the overall impedance behavior, and that differences in geometry, A-K gap spacings, and cathode dimensions can have a large influence over the diode's impedance profile [12]. These experiments are designed to help to verify the simulation results, as well as provide input parameters and limits for the simulations with respect to species, densities, and temperatures.

III. Diagnostics and Results

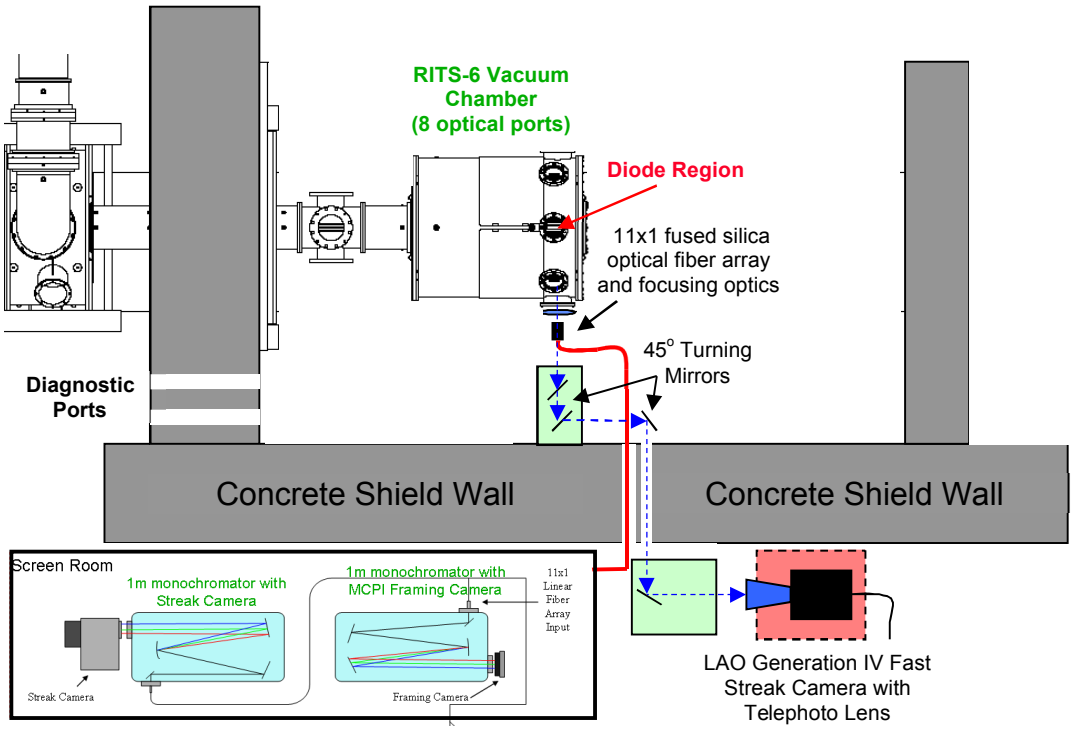

Figure 3. Optical diagnostic layout at RITS.

Figure 3 shows the diagnostic layout around the RITS accelerator. The majority of the diagnostics are positioned outside of the RITS test cell (cement wall enclosure area) to limit their exposure to hard x-rays and electromagnetic pulses (EMP). Light is collected through lenses focused into the center of the vacuum chamber and transmitted to the different diagnostics using either mirrors or fiber optics. The three primary diagnostics described here are the optical imaging streak camera system (ISS), the optical spectroscopy system, and the avalanche photodiode detector arrays.

A. Streak camera

The streak camera is custom built by NSTec Los Alamos operations using commercial components [13]. The camera consists of a Photonis P510 streak tube, S-20 photocathode, and P-22 aluminized phosphor output screen. It is attached to a Princeton Instruments Quad-Pro CCD, with a large format, 50mm array readout. The camera is capable of continuously

selectable sweep rates from 20ns to 500µsec with high spatial resolution (10 lp/mm). For these experiments, the streak camera was fielded in two orientations, looking at electrode plasma expansion in time. Figure 4 shows an image taken with the camera oriented to view across the A-K vacuum gap.

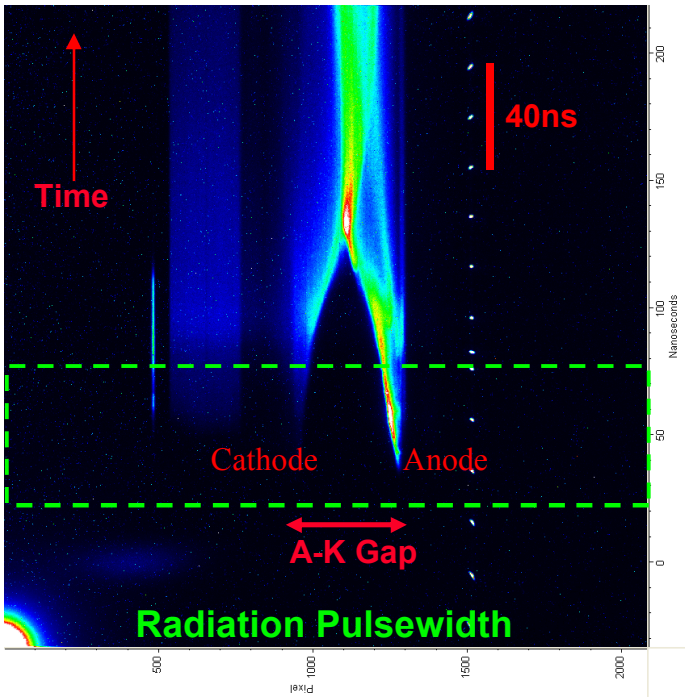

Figure 4. Optical streak camera image showing plasma propagation across the A-K gap.

Some features of the image are the 20ns timing markers on the right, and a scintillation fiber on the left which corresponds to the x-ray radiation pulse (not time corrected in the image). The green dashed lines indicate the radiation pulsewidth (FWFM), and the A-K gap is identified. As can be seen, plasmas begin on the anode and cathode electrodes, and move towards the center where they meet about 50ns after the radiation pulse. These plasma are indicative of the higher density (1x10^17 cm-3) electrode plasmas modeled in LSF (see figure 13). Figure 5 shows the same image with the camera oriented to view radially across the A-K gap. In this image taken just off the anode surface, we see a bright region of plasma which corresponds to the focal spot of the beam. The plasma expands radially during the radiation pulse. The intensity of the plasma decreases following the radiation pulse and expands outward to cover

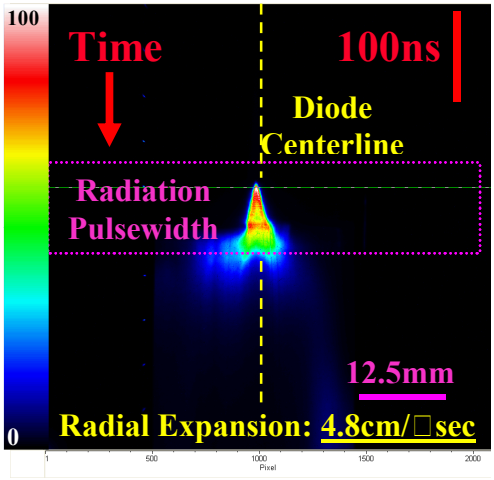

Figure 5. Optical streak camera image showing radial plasma distribution in-front of the anode surface.

the entire extent of the camera's view. Similar images were taken at different axial positions across the A-K gap. These images provide an estimate of the anode and cathode plasma expansion velocities of 5-10 cm/μsec, with the anode plasma expansion rate being approximately twice that of the cathode. This compares well with values obtained from LSP simulations of the anode plasma expansion velocities of 10 cm/μsec [12].

B. Avalanche Photodetectors

A bank of eight silicon avalanche PIN photodetectors (APDs) is used to look at the plasma light evolution across the A-K gap. These detectors are custom built by NSTec Los Alamos operations using commercial Hamamatsu APD detectors [14]. These detectors have a fast (nanosecond) response time, high quantum efficiency, and high gain. They are ideal for looking at lower density ($1x10^{14}$ cm^{-3}) plasmas which are present in the diode during the radiation pulse. Figure 6 shows the APD responses at different axial positions from the anode for a typical SMP diode shot. The plasma light rapidly increases in intensity and goes off-scale; however, during the radiation pulse the detectors pick-up lower level light emission out in the vacuum gap, which is consistent with simulations [12]. In simulations, this light intensity is from plasmas with densities on the order of 10^{15}-10^{16} cm^{-3}. Figure 7 shows a series of shots where the APDs were used to measure the expansion velocity of the anode and cathode plasmas.

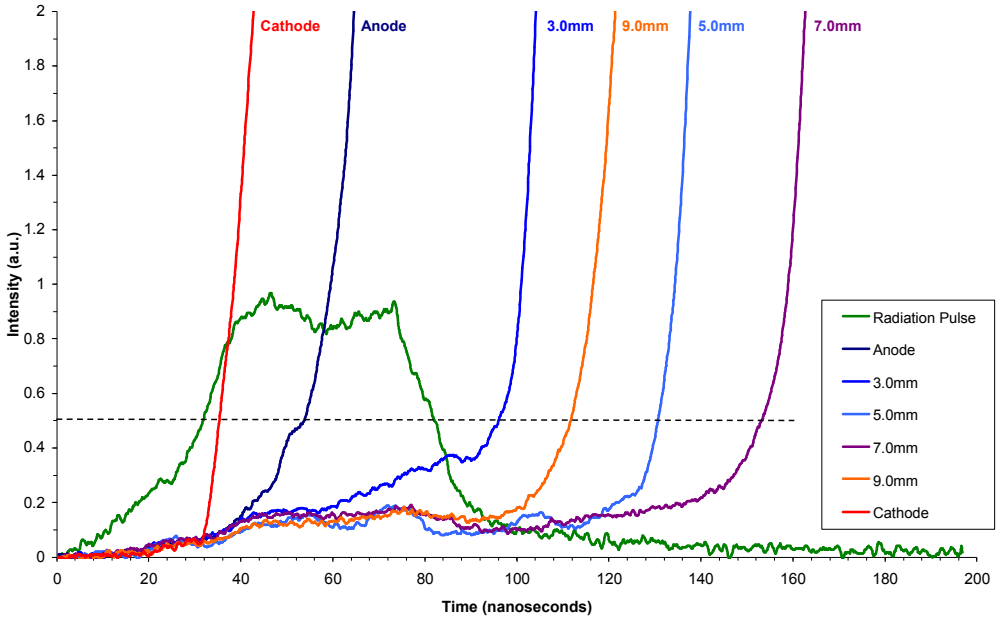

Figure 6. Avalanche photodetector signals for typical SMP shot.

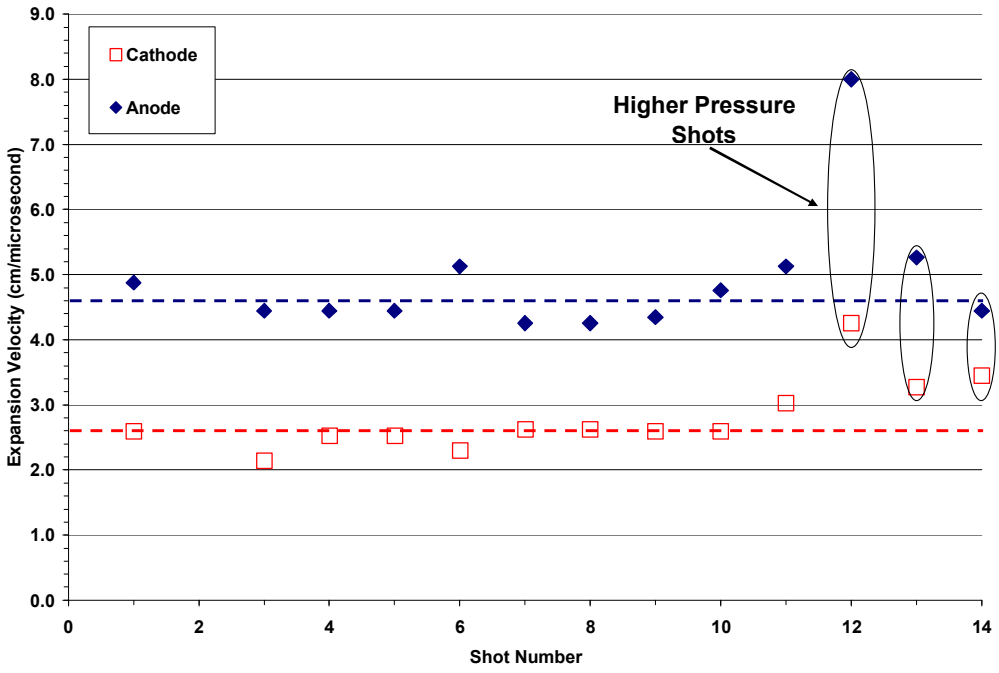

Figure 7. Cathode and anode plasma expansion velocities for a series of SMP shots.

The difference in time between the fibers at the 0.5 reference intensity level (the beginning of the sharp-rise portion in figure 6) is used to measure the electrode expansion velocities. Using this

method, the average anode expansion velocity over all the shots is 4.6 +/- 0.3 cm/μsec, while the cathode expansion rate is 2.6 +/- 0.2 cm/μsec. Again the anode velocity is nearly twice that of the cathode, consistent with the streak camera data. The last three shots plotted on the graph were taken at an order of magnitude higher base pressures than the usual $1x10^{-5}$ Torr. It is interesting to note that manipulating the background gas pressure appears to have an effect on the plasma expansion rates. While it is not necessarily intuitive that the expansion rates should increase at higher pressures, the results are consistent with LSP simulations that indicate this result is due to the larger contaminant inventory on the electrode surfaces at the higher pressures.

C. Spectroscopy

Optical spectra were collected on the SMP diode plasmas using a 150mm Acton spectrometer with a Princeton Instrument PI-Max ICCD camera at the output. Light was collected from inside the chamber through an achromat lens onto an 11 x 1 array composed of 200 micron diameter fused silica optical fibers. The fibers transmit the light 10 meters into the RITS shielded screenroom outside of the RITS test cell area. The fibers were oriented radially at different axial location across the A-K gap. Figure 8 shows an example of how the array was oriented along with an image of the spectra.

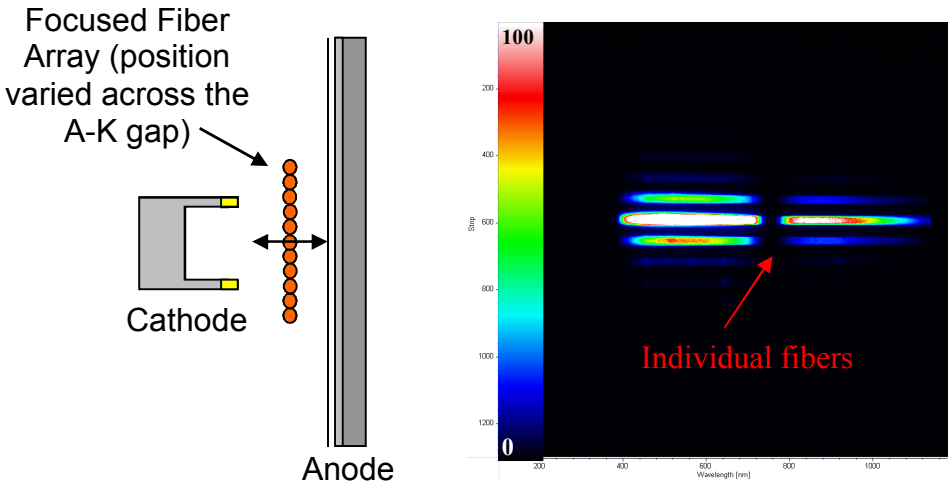

Figure 8. Visible spectra of the SMP diode.

This image was taken just off the anode surface during the mid-portion of the radiation pulse (see figure 10). Due to the large variation in intensity levels between the fibers, it is difficult to see the details on the outer fibers. Figure 9 shows the individual lineouts for the fibers in Figure 8. This plot is given on a log scale to effectively show the difference in intensity levels between the fibers (three orders of magnitude).

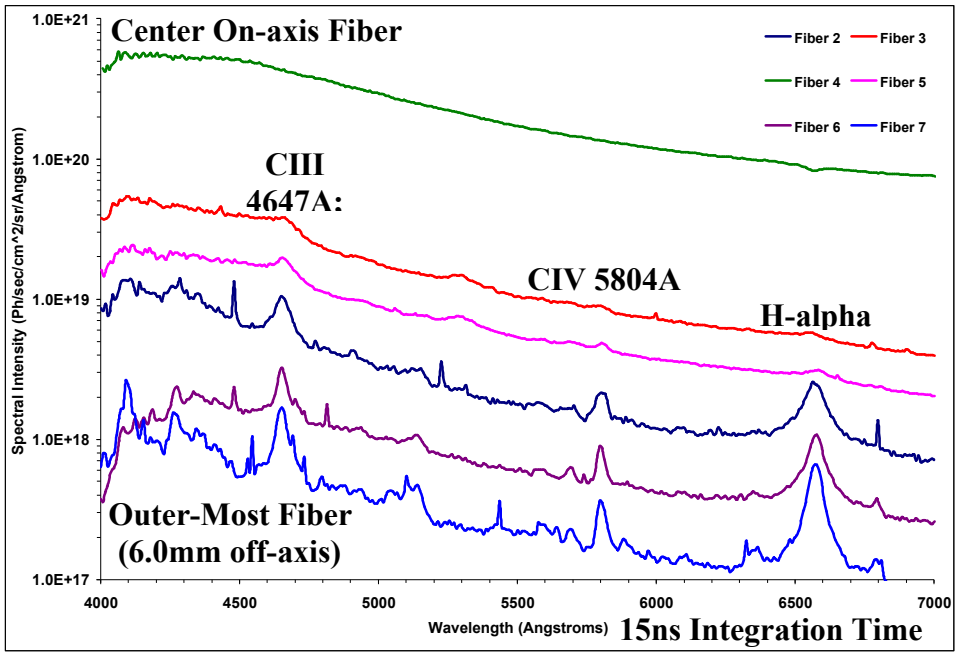

Figure 9. Spectral lineouts for SMP diode on RITS.

The dominant lines in the spectrum are from neutral hydrogen, and doubly and triply ionized carbon. In addition, smaller features from oxygen and aluminum are also present. All of the spectra are calibrated in absolute intensity units, following the procedure detailed in reference 15.

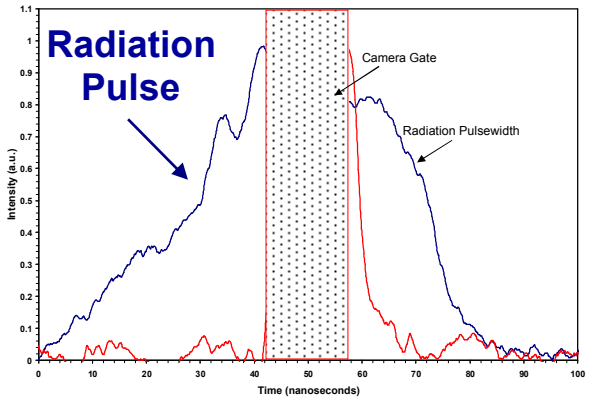

Figure 10. Spectral gate-time relative to radiation pulse.

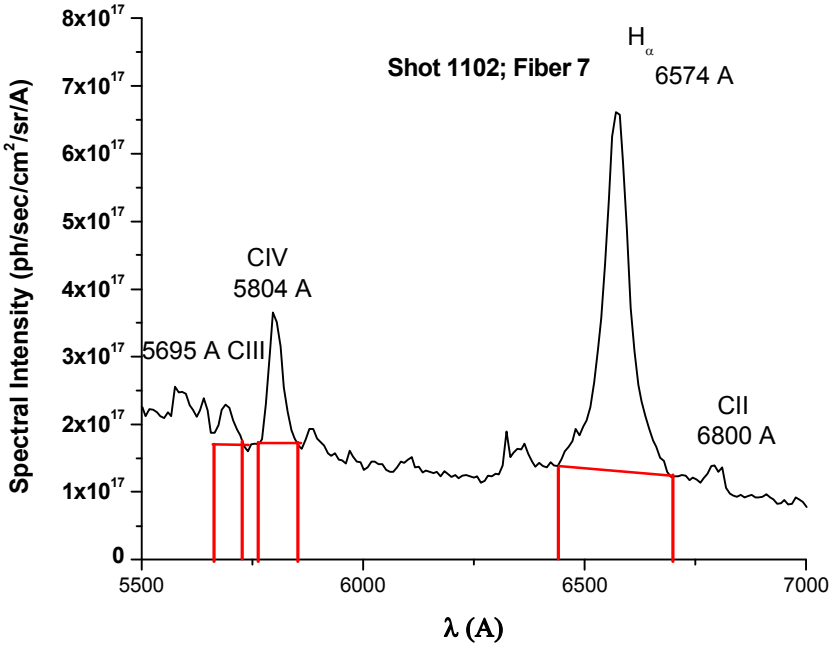

Figure 11. Spectral lineout of SMP diode shot.

The spectra are analyzed using line shape, time-dependent, and collisional-radiative (CR) calculations [16-18]. Different chordal lines of sight are considered for each of the fibers, with the plasma volumes being inferred from the streak camera images and APD data. Due to low ion temperatures (<10eV), the measured line widths are only due to the instrumental resolution and the local Stark broadening. The Stark broadening FWHM (Lorentzian) is deconvolved from the Voigt profile for the line [19]. Fits for the continuum radiation in the spectra were made in order

to determine the line intensities (by subtracting the continuum), and to determine the electron density from the absolute continuum intensity. Figure 11 shows a close-up of the bottom lineout in figure 10. In this figure, the hydrogen H_α line broadening is 41 Angstroms, which gives a local electron density (N_e) of 7.4×10^{17} cm^{-3}, in contrast to the electron density obtained from the absolute continuum which gives a line-averaged density of 2.9×10^{17} cm^{-3}. The difference in densities indicates that the hydrogen is localized within only a portion of the full line of sight of the fiber. The ratio of the CIII (5696 A) to CIV (5804 A) lines gives the electron temperature (T_e). Figure 12 shows the dependence of this ratio with temperature. For the ratio in Figure 11, the electron temperature is determined to be 5.2eV.

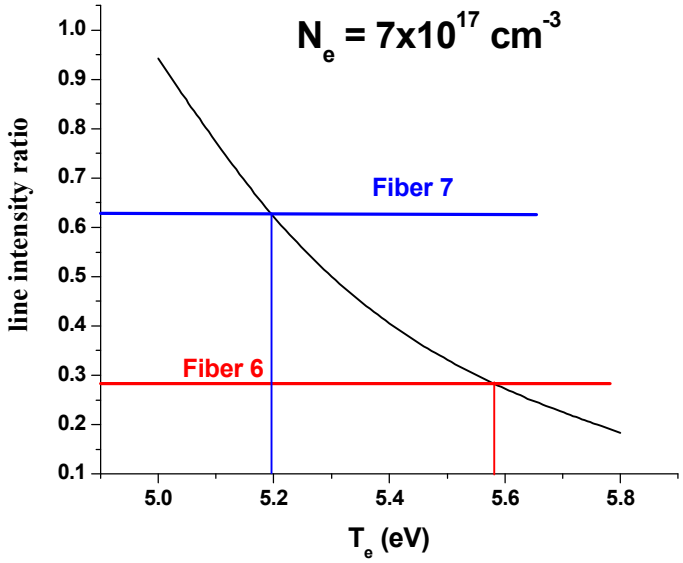

Figure 12. CIII/CIV line ratio electron temperature plot (steady state calculations).

Using the absolute intensities of the hydrogen H_α (6563 A) and the CIV (5804 A) absolute line intensities, one can obtain the number densities for hydrogen and carbon. These number densities are then compared with the total electron density, with the remaining electron density being due to other species such as oxygen and aluminum. At these temperatures (< 10eV) and densities, the opacities of the carbon lines are small, such that the plasma can be considered to be optically thin for the lines considered. Table 1 provides a summary of all the plasma parameters for the spectra in Figure 10. Similar analyses are being done for the other lineouts in

N_e from H_α	**7.4×10^{17} cm^{-3}**
N_e from continuum	**2.9×10^{17} cm^{-3}**
Electron Temp. (T_e)	**5.2 eV**
$N_{hydrogen}$ (Z = 1)	**3.2×10^{17} cm^{-3} (45%)**
N_{carbon} (Z = 2.9)	**3.0×10^{16} cm^{-3} (12%)**
$N_{e(other)}$	**3.0×10^{17} cm^{-3} (43%)**

Table 1. Summary of plasma parameters.

figure 9, as well as other spectra taken at different axial locations. The goal of this work is to reconstruct a density and temperature profile similar to that generated by the LSP simulations, as shown in figure 13. This work is ongoing and will be given in a future publication.

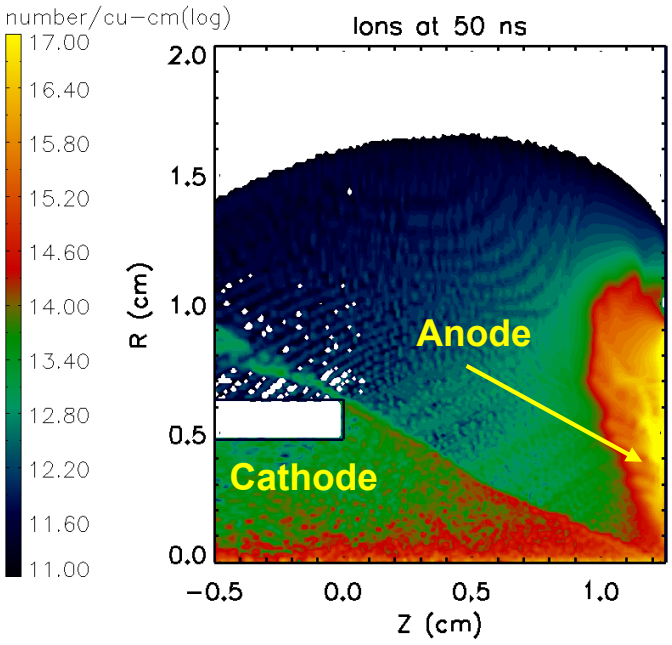

Figure 13. Simulation of the anode plasma C+ species at 50 ns.

To summarize the spectroscopy results, the electron temperature, density, and plasma uniformity decrease radially moving out from the central axis. In addition, the fraction of electrons from species other than carbon and hydrogen decreases as one moves away from the axis, which is likely due to the finite monolayers of contaminants present on the surface. Once the surface contaminant monolayers are extinguished by the beam, the base metal contributes more to the plasma. Since the base metal is aluminum, which also has a substantial oxide layer, hydrocarbons, oxygen and aluminum species become prevalent. The high plasma density on-axis leads to excessive broadening of the lines (see figure 9), to the extent that individual line species become indistinguishable from the continuum. Since these species are assumed to be present within the spectrum, they contribute to the overall lineshape of the continuum, making temperature determinations difficult. Accurately determining the temperatures from the continuum shape is ongoing work. Finally, it is noteworthy to point out that since the spectra are collected radially on both sides of the central axis, information is gathered on the symmetry of the diode plasma as well.

IV Summary:

A series of shots were taken on the self-magnetic pinch (SMP) electron beam diode on the RITS-6 accelerator at Sandia National Laboratories. Plasma diagnostics, including: optical streak imaging, spectroscopy, and photon detection, were used to characterize the electrode plasmas both spatially and temporally within the A-K vacuum gap region. Dense plasmas (>10^17cm-3) observed on the electrodes propagate out into the vacuum gap with expansion rates of 5-10 cm/μsec during the course of the 45nsec radiation pulse. It is believed that these plasmas are responsible for the gradual (0.5 Ohms/nanosecond) impedance decay of the diode which is observed both experimentally and in simulations. The results of these experiments are incorporated into hybrid, particle-in-cell / fluid dynamic codes to design the next generation of enhanced radiographic sources.

Acknowledgment:

Sandia National Laboratories is a multi-program laboratory managed and operated by Sandia Corporation, a wholly owned subsidiary of Lockheed Martin Corporation, for the U.S. Department of Energy's National Nuclear Security Administration under contract DE-AC04-94AL85000.

References:

1. D. Johnson, V. Bailey, R. Altes, P. Corcoran**,** *et al*., "Status of the 10MV, 120kA RITS-6 Inductive Voltage Adder," Proceedings of the 15th IEEE International Pulsed Power Conference, 314 (2007).

2. K. Hahn, N. Bruner, M.D. Johnston, B.V. Oliver, *et al*., "Overview of the Self-Magnetic Pinch Diode Investigations on RITS-6," IEEE Trans. on Plasma Science, 38, 2652 (2010).

3. A.E. Blaugrund and G. Cooperstein, "Intense Focusing of Relativistic Electrons by Collapsing Hollow Beams," Phys. Rev. Letters, 34, 461 (1975).

4. S.B. Swanekamp, G. Cooperstein, J.W. Schumer, D. Mosher, *et al*., "Evaluation of Self-Magnetically Pinched Diodes up to 10MV as High-Resolution Flash X-ray Sources," IEEE Trans. on Plasma Science, 32, 2004 (2004).

5. D.D. Hinshelwood, G. Cooperstein, D. Mosher, D.M. Ponce, *et al*., "Characterization of a Self-Magnetic-Pinched Diode," IEEE Trans. on Plasma Science, 33, 696 (2005).

6. D.D. Hinshelwood, R.J. Allen, R.J. Commisso, G. Cooperstein, *et al*., "High-Power Self-Pinch Diode Experiments for Radiographic Applications," IEEE Trans. on Plasma Science, 35, 565 (2007).

7. A.E. Blaugrund, G. Cooperstein, "Relativistic Electron Beam Pinch Formation Processes in Low Impedance Diodes," Phys. of Fluids, 20, 1185 (1977).

8. J.E. Maenchen, G. Cooperstein, J. O'Malley, and I. Smith, "Advances in Pulsed Power-Driven Radiography Systems," Proc. IEEE, 92, 1021, (2004).

9. M.E. Cuneo, "The Effect of Electrode Contamination, Cleaning, and Conditioning on High-Energy, Pulsed Power Device Performance," IEEE Trans. Dielectric Electrical Insulation, 6, 469 (1999).

10. J.O'Malley, J. Maenchen, and G. Cooperstein, "Status of Diode Research Programme at AWE," Proc. 14th IEEE International Pulsed-Power Conference, Dallas, TX, June 15-18, 2003, vo.1, p.21-28.

11. LSP is a software product of ATK Mission Research

12. N. Bruner, D.R. Welch, K.D. Hahn, and B.V. Oliver, *Phys. Rev. ST Accel. Beams*, Vol. 14, 024401 (2011).

13. A. Lewis and C. Hollabaugh, *Proc. SPIE 6294, Infrared and Photoelectronic Imagers and Detector Devices II*, p. 629405, (September 07, 2006).

14. NSTec Los Alamos Operations, 1072 Cheyenne St. Los Alamos, NM 87544.

15. M.D. Johnston, B.V. Oliver, D.W. Droemer, B. Frogget, et al., *Review of Sci. Instruments*, Vol. 83, No. 8, p. 083108-1.

16. E. Stambulchik and Y. Maron, "A Study of Ion-Dynamics and Correlation Effects for Spectral Line Broadening in Plasma: K-shell Lines," Journal of Quantitative Spectroscopy & Radiative Transfer, 99, 730 (2006).

17. E. Stambulchik and Y. Maron, "Stark Effect in High-n Hydrogen-like Transitions," Journal of Physics B. 41, 095703 (2008).

18. Yuri V. Ralchenko and Y. Maron, "Accelerated Recombination Due to Resonant Deexcitation of Metastable States," Journal of Quantitative Spectrscopy & Radiative Transfer, 71, 609 (2001).

19. E.E. Whiting, "An Empirical Approximation to the Voight Profile," *J. Quantitative Spectroscopy and Radiative Transfer*, Vol. 8, p. 1379 (1968)